Ventricular Conduction System Modeling for Electrophysiological Simulation of the Porcine Heart

Ricardo M Rosales[1,2], Konstantinos A Mountris[3], Manuel Doblaré[1,2], Manuel M Mazo[4,5], Esther Pueyo[1,2]

[1] Aragon Institute of Engineering Research, University of Zaragoza, IIS Aragón, Zaragoza, Spain
[2] CIBER de Bioingeniería, Biomateriales y Nanomedicina, Instituto de Salud Carlos III , Spain
[3] Mechanical Engineering, University College London, London, United Kingdom
[4] Regenerative Medicine Program, CIMA Universidad de Navarra, Pamplona, Spain
[5] Hematology and Cell Therapy, Clínica Universidad de Navarra, Pamplona, Spain

Abstract

Depolarization sequences triggering mechanical contraction of the heart are largely determined by the cardiac conduction system (CS). Many biophysical models of cardiac electrophysiology still have poor representations of the CS. This work proposes a semiautomatic method for the generation of an anatomically-realistic porcine CS that reproduces ventricular activation properties in swine computational models.

Personalized swine biventricular models were built from magnetic resonance images. Electrical propagation was described by the monodomain model. The CS was defined from manually-determined anatomic landmarks using geodesic paths and a fractal tree algorithm. Two CS distributions were defined, one restricted to the subendocardium and another one by performing a subendo-to-intramyocardium projection based on histological porcine data. Depolarization patterns as well as left ventricular transmural and inter-ventricular delays were assessed to describe ventricular activation by the two CS distributions.

The electrical excitations calculated using the two CS distributions were in good agreement with reported activation patterns. The pig-specific subendo-intramyocardial CS led to improved reproduction of experimental activation delays in ventricular endocardium and epicardium.

1. Introduction

In silico modeling and simulation have become powerful tools to gain insight into cardiac electrical activity. In silico representation of the cardiac conduction system (CS) arises as a vital step in cardiac electrophysiology, as it determines the ventricular activation sequence that triggers mechanical contraction to pump blood throughout the body. Several CS computational descriptions have been proposed, most of them grounded on reported histological images or aimed at reproducing physiological and pathological excitation patterns including, among the latter, retrograde conduction and life-threatening arrhythmias [1, 2].

While relevant advances have been made in the species-specific or patient-specific mathematical representation of cardiac ion kinetics, ventricular anatomies and fiber orientation fields, modeling of the CS and its connection with the ventricular myocardium is not so well developed, particularly in pigs, which are commonly used due to their similarity to humans in terms of ventricular electrophysiology. The infeasibility to acquire personalized in vivo CS data encourages computational definitions of CS using mathematical algorithms seeking to replicate available experimental evidence [3].

This work develops semiautomatic methods to generate a CS representation that accurately reproduces depolarization patterns in computational models of healthy pig ventricles, with the generated CS being species-specific and anatomically-realistic. Porcine-specific biventricular geometries and fiber fields were determined from diffusion-weighted magnetic resonance images (DW-MRI). Transmural heterogeneities were defined by solving a Dirichlet-Laplace problem in the biventricular domain [4]. Two different CS distributions were evaluated, one restricted to the subendocardium and another one involving deeper intramyocardial projection. Validation was performed by calculating activation times (ATs) and comparing with experimentally available depolarizing patterns.

2. Materials and Methods

2.1. Modeling and Simulation

Ex vivo DW-MRI were obtained from three porcine samples while preserving cardiac volume and avoiding

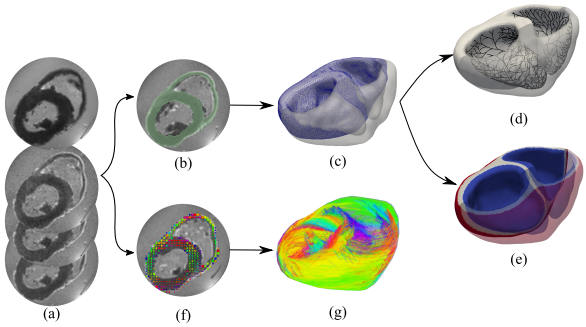

Figure 1: Modeling pipeline. (a) Diffusion images. Baseline and three gradients are depicted. (b) Segmentation. (c) Volume discretization. (d) CS computation. (e) Transmural heterogeneity, with endo-, mid- and epicardium depicted in blue, white and red, respectively. (f) Per-slice diffusion tensor estimations shown by colored glyphs. (g) Tractography determination.

chambers collapse. Figure 1 shows the modeling pipeline used to create realistic biventricular computational models based on processing of ex vivo data.

First, a semi-automatic approach was used to segment the ventricular myocardium. The three-dimensional (3D) segmentation was discretized by irregular tetrahedral elements with maximum volume of $0.1\,\mathrm{mm}^3$ employing the *iso2mesh* framework [5]. Due to ventricular thickness inhomogeneity, a multi-diffusion analysis was used to segment the myocardium transmurally. Following the method proposed in [4], the Laplace equation was solved with distinct epicardial and left and right endocardial Dirichlet boundary conditions as well as a zero-flux Neumann boundary condition on the base of the heart. Thresholds were set to define endo-, mid- and epicardial layers with a transmural proportion of 0.4, 0.35 and 0.25, respectively.

Cardiac DW-MRI was acquired with 16 directional electromagnetic gradients for pig 1 and 64 for pigs 2 and 3, enabling the estimation of the diffusivity function as a positive-valued Cartesian tensor with even order and full symmetry [6]. The direction with major water diffusivity in a voxel, which corresponds to the diffusion tensor eigenvector in that spatial location, was assigned as the longitudinal fiber direction.

Electrophysiological propagation in ventricular tissue was described by the monodomain model. The O'Hara-Rudy model [7] was employed to represent the cellular action potential of the endo-, mid- and epicardium, while CS cellular electrophysiology was defined by the Stewart model [8]. The reaction-diffusion equation was solved using the in-house developed software *ELECTRA* [9–11]. A method that dynamically selects the time integration step allowing an explicit derivative computation with the forward Euler method in the time domain was used. The finite element method was employed for the numerical resolution of the spatial derivatives.

An orthotropic diffusivity with transverse isotropy was considered for modeling the ventricular domain. Ventricular longitudinal diffusivity was set to $0.0013\,\mathrm{cm}^2/\mathrm{ms}$ with a transverse-to-longitudinal diffusivity ratio of 0.25, which matches the reported anisotropy in cardiac conduction velocity [12]. The longitudinal diffusivity of the CS was set to $0.01\,\mathrm{cm}^2/\mathrm{ms}$ and decremented around the Purkinje-myocardial junction (PMJ) to match ventricular diffusion using a Boltzmann curve as in [1].

All cellular models were individually simulated for $1000\,\mathrm{s}$ to reach a stable action potential duration. Each biventricular simulation consisted of two $1\,\mathrm{Hz}$-paced cycles, with the second cycle being used for AT calculation. Stimuli of $80\,\mathrm{mA}$-magnitude and $1\,\mathrm{ms}$-duration were applied at the atrioventricular node (AVN). PMJ-activated ventricular nodes were located at a maximum distance of $1\,\mathrm{mm}$ from the CS.

2.2. Conduction System Determination

The CS mesh was generated by connecting manually located landmarks with one-dimensional elements in the 3D space. First, the AVN was positioned $5\,\mathrm{mm}$ above the septal base towards the anterior right ventricle (RV). The His bundle continued with a straight line until the septum, where a bifurcation originated the left and right branches, both of which traveled straight until the left and right basal endocardium of the septum, respectively, as shown in Figure 2a. The branches grew from base to apex through geodesic paths computed in the endocardial meshes. The left one ramified into the anterior and posterior left branches whilst the right one developed parallel to the endocardial surface, ending in the anterior RV. The three branches ended in the insertion of the papillary muscles at nearly one third in the apico-basal direction.

The Purkinje tree was delineated from the endpoints of the three bundle branches with a fractal tree algorithm and projected onto the endocardial surfaces, as reported in [3]. Both ventricles contained regularly distributed PMJs except for the basal area and the posterior RV. This CS distribution where the projection only reached subendocardial tissue was denominated *subendocardial CS* (s-CS). In addition, a more porcine-specific *intramyocardial CS* (i-CS) was defined by including a deeper projection onto the ventricular walls according to histological observations from [13]. To build the i-CS, the diffusion scalar maps and the mid-myocardial boundaries previously established when setting the transmural heterogeneities were considered to define the subendo- and intramyocardial ventricular regions, as depicted in Figure 2b. The subendocardial region (S) was computed as the outermost half of the endocardium while the intramyocardial region (I) was defined

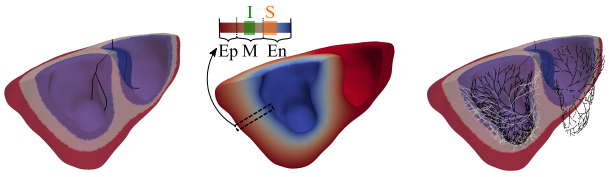

(a) (b) (c)

Figure 2: (a) In silico His bundle with left anterior, left posterior and right branches. (b) The LV transmural layers and its diffusion scalar map calculated solving a Dirichlet-Laplace problem are depicted, with Ep: epi, M: mid, En: endo, I: intramyo and S: subendo. (c) s-CS and i-CS for pig 2 shown in black and white, respectively.

as the middle third of the mid-myocardium. The projection was performed in two steps. In the first one, every CS node was projected onto S except for the right Purkinje tree. The projection magnitude for a CS node was computed as its mean distance with the 5 nearest subendocardial nodes while its projection direction was obtained as the mean normal direction of the 15 nearest myocardial nodes at the endocardial surface. In the second step, 75 % of the CS ending branches in the left ventricle (LV) were further projected onto I, as shown in Figure 2c. The ending node of a CS ending branch CS_{eb} was assigned a projection direction CS_{ebd} and magnitude CS_{ebm} as described above. Then, the CS_{eb} nodes were relocated by setting the fixed CS_{ebd} direction and by linearly varying their projection magnitudes from zero to CS_{ebm} for the joint and ending nodes, respectively. To avoid sharp orientation changes in the projected CS mesh, the maximum angle between two segments was constrained to $\pm 20°$.

2.3. Activation Characterization

Simulated myocardial ATs for both CS distributions were compared against experimental activation patterns including descriptions of initial excitation, first epicardial breakthrough and final epicardial depolarization for both ventricles [14, 15]. Moreover, ventricular delays were calculated as in [16]. The inter-ventricular delay (IVD) was computed as the difference between the earliest AT in LV and RV epicardium.

The LV transmural delay (LVTD) was calculated as the difference between the earliest AT in LV epicardium and endocardium. The computed delays were compared to corresponding experimental values reported for porcine [16] and human ventricles [14, 15].

3. Results and Discussion

The i-CS distribution yielded lower ATs than the s-CS distribution for the three simulated porcine ventricles. This

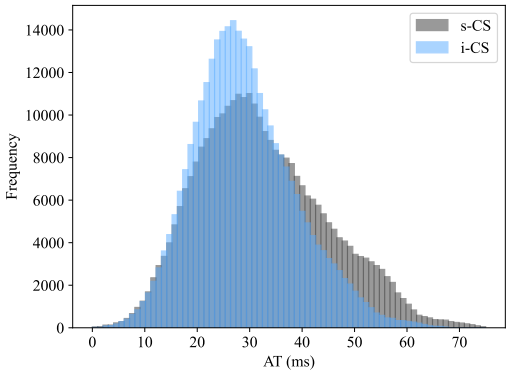

Figure 3: Histogram of ATs calculated for s-CS and i-CS distributions in simulated pig 1.

is illustrated for simulated pig 1 in Figure 3.

The excitation was initiated between 2 and 4 ms earlier in the LV than in the RV for the s-CS, which agreed with the early LV depolarization reported in [14]. For the i-CS, these time differences were reduced by 1 ms with respect to the s-CS. The pattern of excitation initiation was the same as for the s-CS, except for pig 2 where the starting excitation occurred simultaneously in both ventricles.

For both s-CS and i-CS, the first epicardial breakthrough was found at the apex and pretrabecularis area of the RV, presumably due to the thinner wall of the RV. Specifically, the pretrabecularis area was activated in the range of 16 to 27 ms for the s-CS, while for the i-CS this range was slightly lower, from 15 to 25 ms, which better replicates the 7 to 25 ms experimental range shown in [15].

The depolarization waves within each ventricle ended in the postero-basal area for both LV and RV regardless of the CS distribution, which resembled experimentally reported depolarization patterns. Maximum ATs were located at the postero-basal RV in all biventricular geometries and were found to diminish from 75, 97 and 87 ms for the s-CS to 67, 93 and 86 ms for the i-CS for simulated pigs 1, 2 and 3, respectively, thus resulting in better agreement with the values described in [14].

Simulated IVD and LVTD values for the two tested CS distributions are shown in Table 1. The i-CS allowed better reproduction of the swine experimental mean LVTD of 11 ms reported in [16]. LVTD decremented from a mean value of 36 ms for the s-CS to 22.3 ms for the i-CS over the three pig ventricular models. Similarly, the simulated mean IVD was reduced from 21.3 for s-CS to 15 ms for i-CS, better approximating the mean IVD delays of 12.4 and 5.4 ms reported experimentally in humans [15] and pigs [16], respectively. The three simulated pigs showed a reduction in the activation delays for i-CS as compared to s-CS, with the largest differences observed for simulated

Table 1: Inter-ventricular, IVD, and transmural, LVTD, activation delays for s-CS and i-CS distributions.

	Pig1		Pig2		Pig3	
	s-CS	i-CS	s-CS	i-CS	s-CS	i-CS
LVTD (ms)	27	9	53	40	28	18
IVD (ms)	14	4	35	30	15	11

pig 1 which might be caused by a thinner LV in this case.

4. Conclusion

This work proposes a method for in silico definition of pig-specific CS that departs from a subendocardial CS representation, s-CS, and performs a subendo-to-intramyocardium projection based on porcine histology data to obtain an i-CS representation. In pig-specific biventricular models, both CS representations reproduced the expected depolarization sequence, with i-CS better replicating the RV epicardial ATs in the pretrabecularis area. Also, simulated transmural and inter-ventricular delays were in better agreement with experimental values when calculated with i-CS than with s-CS.

Acknowledgments

This work was supported by the European Research Council under G.A. 638284, by EU H2020 under G.A. 874827 (BRAV3) and Marie Skłodowska-Curie G.A. 101024463 (PhyNeTouch), by Ministerio de Ciencia e Innovación (Spain) through project PID2019-105674RB-I00 and by European Social Fund (EU) and Aragón Government through group T39_20R and project LMP94_21.

References

[1] Dux-Santoy L, Sebastian R, Rodriguez JF, Ferrero JM. Modeling the Different Sections of the Cardiac Conduction System to Obtain Realistic Electrocardiograms. In 2013 35th Annual Int Conf of the IEEE Engin in Med and Biol Soc (EMBC). Osaka: IEEE, 2013; 6846–6849.

[2] Sebastian R, Zimmerman V, Romero D, Sanchez-Quintana D, Frangi AF. Characterization and Modeling of the Peripheral Cardiac Conduction System. IEEE Trans Med Imaging 2013;32(1):11.

[3] Sahli Costabal F, Hurtado DE, Kuhl E. Generating Purkinje Networks in the Human Heart. J Biomech 2016; 49(12):2455–2465.

[4] Perotti LE, Krishnamoorthi S, Borgstrom NP, Ennis DB, Klug WS. Regional Segmentation of Ventricular Models to Achieve Repolarization Dispersion in Cardiac Electrophysiology Modeling. Int J Numer Meth Biomed Engng 2015; 31(8):e02718.

[5] Tran AP, Yan S, Fang Q. Improving Model-Based Functional Near-Infrared Spectroscopy Analysis Using Mesh-Based Anatomical and Light-Transport Models. Neurophotonics 2020;7(1):1 – 18.

[6] Barmpoutis A, Vemuri BC. A Unified Framework for Estimating Diffusion Tensors of Any Order with Symmetric Positive-Definite Constraints. In 2010 IEEE Int Symp Biomed Imaging: From Nano to Macro. 2010; 1385–1388.

[7] O'Hara T, Virág L, Varró A, Rudy Y. Simulation of the Undiseased Human Cardiac Ventricular Action Potential: Model Formulation and Experimental Validation. PLoS Comput Biol 2011;7(5):e1002061.

[8] Stewart P, Aslanidi OV, Noble D, Noble PJ, Boyett MR, Zhang H. Mathematical Models of the Electrical Action Potential of Purkinje Fibre Cells. Phil Trans R Soc A 2009; 367(1896):2225–2255.

[9] Mountris KA, Dong L, Guan Y, Atluri SN, Pueyo E. Meshfree Implementation of the Cardiac Monodomain Model Through the Fragile Points Method. J Comput Sci 2022; Under review.

[10] Mountris KA, Pueyo E. A Dual Adaptive Explicit Time Integration Algorithm for Efficiently Solving the Cardiac Monodomain Equation. Int J Numer Method Biomed Eng 2021;37(7):e3461.

[11] Mountris KA, Pueyo E. The Radial Point Interpolation Mixed Collocation (RPIMC) Method for the Solution of the Reaction-Diffusion Equation in Cardiac Electrophysiology. In Int Conf Comput Exper Eng Sci. Springer, 2021; 39–44.

[12] Spach MS, Miller WT, Geselowitz DB, Barr RC, Kootsey JM, Johnson EA. The Discontinuous Nature of Propagation in Normal Canine Cardiac Muscle. Evidence for Recurrent Discontinuities of Intracellular Resistance that Affect the Membrane Currents. Circ Res 1981;48(1):39–54.

[13] Garcia-Bustos V, Sebastian R, Izquierdo M, Rios-Navarro C, Bodí V, Chorro FJ, Ruiz-Sauri A. Changes in the Spatial Distribution of the Purkinje Network After Acute Myocardial Infarction in the Pig. PLoS ONE 2019;14(2):e0212096.

[14] Durrer D, Van Dam RT, Freud GE, Janse MJ, Meijler FL, Arzbaecher RC. Total Excitation of the Isolated Human Heart. Circulation 1970;41(6):899–912.

[15] Wyndham CR, Meeran MK, Smith T, Saxena A, Engelman RM, Levitsky S, Rosen KM. Epicardial Activation of the Intact Human Heart Without Conduction Defect. Circulation 1979;59(1):161–168.

[16] Soto Iglesias D, Duchateau N, Kostantyn Butakov CB, Andreu D, Fernandez-Armenta J, Bijnens B, Berruezo A, Sitges M, Camara O. Quantitative Analysis of Electro-Anatomical Maps: Application to an Experimental Model of Left Bundle Branch Block/Cardiac Resynchronization Therapy. IEEE J Transl Eng Health Med 2017;5:1–15.

Address for correspondence:

Ricardo M. Rosales

University of Zaragoza, Campus Río Ebro, I+D Building, D-5.01.1B, Mariano Esquillor, s/n street, 50018, Zaragoza, Spain

rrosales@unizar.es